AGU100 ADVANCING EARTH AND SPACE SCIENCE

Water Resources Research

RESEARCH ARTICLE
10.1029/2018WR023884

Key Points:
- We produced new granular information (1-km resolution) on evaporation across California using the biophysical model, Breathing Earth System Simulator
- Annual variations in evaporation were highly damped (393 mm/year +/− 5%) relative to the booms and busts in rainfall between 2001 and 2017 (+/− 28%)
- Statewide evaporation is not increasing with global warming, over 17 years of inspection, because feedbacks dampen the response to a warming climate

Supporting Information:
- Supporting Information S1

Correspondence to:
D. Baldocchi,
baldocchi@berkeley.edu

Citation:
Baldocchi, D., Dralle, D., Jiang, C., & Ryu, Y. (2019). How much water is evaporated across California? A multiyear assessment using a biophysical model forced with satellite remote sensing data. *Water Resources Research*, *55*, 2722–2741. https://doi.org/10.1029/2018WR023884

Received 10 AUG 2018
Accepted 27 FEB 2019
Accepted article online 6 MAR 2019
Published online 5 APR 2019

How Much Water Is Evaporated Across California? A Multiyear Assessment Using a Biophysical Model Forced With Satellite Remote Sensing Data

Dennis Baldocchi[1], David Dralle[2], Chongya Jiang[3], and Youngryel Ryu[3]

[1]Department of Environmental Science, Policy, and Management, University of California, Berkeley, CA, USA, [2]Department of Civil and Environmental Engineering, University of California, Berkeley, CA, USA, [3]Department of Landscape Architecture and Rural Systems Engineering, Seoul National University, Seoul, South Korea

Abstract California is expected to experience great spatial/temporal variations evaporation. These variations arise from strong north-south, east-west gradients in rainfall and vegetation, strong interannual variability in rainfall (±30%) and strong seasonal variability in the supply and demand for moisture. We used the Breathing Earth System Simulator to evaluate the rates and sums of evaporation across California, over the 2001–2017 period. Breathing Earth System Simulator is a bottom-up, biophysical model that couples subroutines that calculate the surface energy balance, photosynthesis, and stomatal conductance. The model is forced with high-resolution remote sensing data (1 km).The questions we address are as follows: How much water is evaporated across the natural and managed ecosystems of California? How much does evaporation vary during the booms and busts in annual rainfall? and Is evaporation increasing with time due to a warming climate? Mean annual evaporation, averaged over the 2001–2017 period, was relatively steady (393 ± 21 mm/year) given the high interannual variation in precipitation (519 ± 140 mm/year). No significant trend in evaporation at the statewide level was detected over this time period, despite a background of a warming climate. Irrigated agricultural crops and orchards, at 1-km scale, use less water than inferred estimates for individual fields. This leaves the potential for sharing water, a scarce resource, more equitably among competing stakeholders, for example, farms, fish, people, and ecosystems.

Plain Language Summary Many stakeholders are contending for the limited water budget that is available to California, the world's fifth largest economy. Yet the amount of water used by natural and managed ecosystems across the state is not well known. We produced a new, process-oriented estimate of statewide water use by natural and managed ecosystems using a biophysical model forced with satellite remote sensing. Despite the booms and busts in rainfall over the 2001 to 2017 period, we find that statewide water use is conservative, compared to the annual variability in rainfall. Nor do we detect that statewide evaporation is increasing as the climate has warmed over this period. We find that crops use less water than conventional wisdom because a subset of fields across a 1-km pixel are fallow and are at peak leaf area and maximum evaporation potential for a relatively short period. Forests, on the other hand, use more water than conventional wisdom because they have a long growing season and absorb more energy than crops. Our intent is to provide water managers with new information on water use to better share water among the various stakeholders, for example, agricultural, cities, fish, ground water reservoirs, and water quality.

1. Introduction

"Whiskey is for Drink'in, Water is for Fight'in Over", attributed to Mark Twain (Samuel Clemens).

In California, water is a relatively scarce, variable, and contentious resource that suffers from intense competition among a diverse set of legitimate stakeholders (farms, cities, terrestrial and aquatic ecosystems, and fish; Hanak et al., 2011). As future conditions warm, California is expected to experience high variability in rainfall as it fluctuates between years with very dry and very wet conditions (Swain et al., 2018). The competition for this water is expected to increase, as evaporation is expected to increase with warming (Anderson et al., 2008).

The sustenance of California's economy, ranked fifth in the world, will depend upon how well this scarce and variable supply of water is shared in a warming and drying world. To use and share this water

effectively and efficiently across a state, these stakeholders will need to know how much water is lost to evaporation from the suite of natural and managed ecosystems and the diverse microclimates that span the state.

If water managers are to divvy up water equitably among farms, fish, forests, and cities in a changing environment (warmer, more CO_2, changing land use, more fires), they need evaporation models with such features as (1) high spatial resolution, (2) high temporal resolution, (3) large area coverage, (4) a capacity for long-term monitoring, and (5) high accuracy (Fisher et al., 2017; Wood et al., 2011). Ideal models should employ biophysical principles at relatively fine time steps (days to weeks) and fine spatial (kilometer or less) scales. The model should consider the biophysical properties of a complicated mosaic of land use, its seasonality, and interannual variability. It is also preferable to evaluate evaporation with biophysical mathematical model that couples water, energy, and carbon fluxes (Baldocchi & Meyers, 1998; Sellers et al., 1997).

California is a challenging test case for applying any bottom-up, biophysical model; California's water balance (evaporation being proportional to precipitation minus runoff minus drainage) is complicated by its diverse geography, ecosystems, microclimates, and land use and land management. What are the key challenges?

First, a competent model must resolve the spatial-temporal variability in meteorological forcing variables. The temperate forests of the Pacific Northwest, the snowy Sierra Nevada, the semiarid grasslands, savannas and chaparrals, the irrigated crops of the Central Valley, and the hot, dry deserts of the south experience vast differences in rainfall, global and net radiation, potential evaporation, vapor pressure humidity deficits, and temperature.

Second, the amount of precipitation varies tenfold across north-south and west-east transects of the state (Iacobellis et al., 2016). We know that from hydroecological theory, there is strong scaling between water availability, primary productivity, and water use (Budyko, 1974; Gentine et al., 2012; Rosenzweig, 1968; Stephenson, 1998). Consequently, a highly variable spatial pattern of actual evaporation is expected to occur across California that reflects this range of precipitation and productivity. We argue that a competent model must resolve the natural gradients in the structure and function of the ecosystems that span the state. It needs information on the structural and functional properties of its vegetation, like leaf area index (LAI), stomatal conductance, and photosynthetic capacity.

Third, the evaluation of much of California's actual evaporation is complicated by the state's wet winter and dry summer, Mediterranean-type climate, which causes an asymmetry in the timing of water supply and demand; water supply is greatest when evaporative demand is least, and vice versa. How native ecosystems use this limited supply of water in a highly demanding environment depends upon how much leaf area they can sustain, how long they can sustain this leaf area, how well they regulate their stomata as the soil dries, how well they establish deeper root systems to access shallow (soil and saprolite) and deep (unsaturated weathered rock and groundwater) pools of moisture, and whether or not they are supplied with irrigation water. Competent biophysical models, that couple carbon, water, and energy exchange, need to consider the seasonality in LAI and physiological capacity to integrate fluxes accurately over a year (Baldocchi & Meyers, 1998; Wang et al., 2007).

Fourth, much year-to-year variability in rainfall is superimposed on this spatial gradient of precipitation and evaporative demand. Climate analyses show that the coefficient of variation of annual rainfall (the ratio between the standard deviation and the mean) ranges between 20% and 70% across the state, placing California among the most variable regions on the continent (Swain et al., 2018); in contrast, the coefficient of variation of rainfall for weather stations east of the Mississippi River is less than 20% (Dettinger et al., 2011). This variable water budget can cause ecosystems to have surplus water during wet years, when they are limited by energy, and evaporate near potential rates. And this variability can cause ecosystems to face severe deficits in their water balances during dry years, forcing them to evaporate at rates much below potential rates.

Fifth, ecosystems in California are experiencing a warmer and drier world (Diffenbaugh et al., 2015). Our more recent heat spells and extended droughts are causing large swaths of mortality of trees in the Sierra Nevada (Asner et al., 2015). Great fires are also occurring across the landscape. A question that remains begging is whether, or not, California ecosystems are experiencing an increase in evaporation over decades and if this increase is exaggerating soil water deficits.

Whether ecosystems experience more or less evaporation with temperature depends on perspective and scale (Jarvis & McNaughton, 1986; Monteith, 1981). From a thermodynamic and physiological perspective, evaporation from leaves and vegetated canopies is expected to increase with warming as it increases the saturation vapor pressure of the surface, thereby increasing the humidity gradient between land and the atmosphere. From a meteorological perspective, warming may decrease evaporation. A warmer surface emits more longwave radiation to the atmosphere, which reduces available energy. In addition, a warmer surface enables more sensible heat to be transferred to the atmosphere, leaving less energy to drive latent heat exchange. When these processes are considered together, a set of feedbacks can act to mute or inhibit the expected positive response of water use by vegetation in a warmer world.

At present, few published water budgets of the state of California exist in the peer-reviewed literature across the spectrum of time and space scales that have been discussed so far. Water budgets for the State that exist tend to infer evaporation as a residual of precipitation and runoff; these budgets are computed at the coarse spatial scales of watersheds (Hanak et al., 2011). Typically, they are averaged over many years, to minimize errors due to changes in storage (Dralle et al., 2018; Draper et al., 2003). Others have focused on the evaporation from agricultural regions of the State (Burt et al., 2002; Sorooshian et al., 2011; Szilagyi & Jozsa, 2018).

Satellite remote sensing provides one way to estimate spatially and temporally integrate evaporation, at relatively small spatial resolution and repeated intervals (Anderson et al., 2007; Hart et al., 2009; Ichii et al., 2009; Jin et al., 2011; Senay et al., 2011; Zhang et al., 2016). Typically, investigators interpret surface energy balance with measurements of thermal infrared radiation or they exploit an empirical link between vegetation indices and surface temperature (Bastiaanssen et al., 1998). There are sets of analyses that have been applied across the nation and world (Jiang & Ryu, 2016; Jung et al., 2011; Mu et al., 2011; Zhang et al., 2010), but none have explicitly extracted information on evaporation across California.

We take a different approach toward evaluating evaporation with biophysical forcing variables from satellite remote sensing. Here we evaluate statewide evaporation with a biophysical model, the *Breathing Earth System Simulator* (BESS). This model calculates evaporation as a balance between the supply and demand for water by coupling submodels that compute energy, water, and carbon fluxes of the land surface (Jiang & Ryu, 2016; Ryu et al., 2011). The model is forced with inputs from satellite remote sensing at high spatial resolution (1 to 5 km).

The BESS model has been tested against a global network of eddy covariance measurements and applied on the global scale against a diverse climate and ecological spaces, like those found in California (Jiang & Ryu, 2016). With its global success, we apply BESS to produce new and unprecedented information on evaporative water use of California at high spatial resolution (1 km) and for nearly two decades.

Based on this background, we ask and answer the following set of questions in this paper. They are as follows: (1) what is the amount of water evaporated across the state of California? (2) how much water is evaporated across major climatic/ecological/agricultural regions of the state, as they experience seasonality in rainfall or irrigation? and (3) how much has annual evaporation varied over the past 17 years, a period that experienced booms and busts in annual rainfall?

Hypotheses we test include the following: (1) year-to-year variability in statewide evaporation is sensitive to booms and busts in rainfall, (2) we are experiencing a positive temporal trend in statewide evaporation due to a warming climate, and (3) water use of irrigated agricultural crops and orchards at 1-km spatial scale may differ from water use measured over individual fields due to the complex mosaic of vegetation and its management.

2. Materials and Methods

2.1. Model Description

Fluxes of water, energy, and carbon dioxide are computed at 1-km spatial resolution on 8-day intervals using the BESS. A full description of the model and its inputs are explained in papers by Ryu et al. (2011) and Jiang and Ryu (2016). Here we provide an abbreviated overview of the model and describe the ingested data products.

BESS relies on the coupling of state-of-the-art biometeorological, physiological, and ecological theory (Baldocchi & Meyers, 1998; Monson & Baldocchi, 2014). Evaporative demand is a function of the

shortwave and longwave radiation balance of the surface and the humidity and temperature of the atmosphere. The supply of water to the atmosphere considers the passage of vapor molecules through the stomata and diffusion out of the soil. This supply is modulated by the surface conductance, which is a function of the LAI of the surface, the sensitivity of stomatal conductance to soil moisture deficits, and the physiological capacity of the vegetation (Baldocchi & Meyers, 1998; Kelliher et al., 1995).

In practice, information on energy exchange and surface temperature are used to evaluate photosynthesis and stomatal conductance of the vegetation. And these variables feedback to evaluate evaporation rates. BESS adopts the quadratic form of the Penman-Monteith equation to compute evaporation (Monteith, 1965; Paw & Gao, 1988). Stomatal conductance is computed as a function of leaf photosynthesis (Farquhar et al., 1980), carbon dioxide concentration, and relative humidity (Ball et al., 1987; Collatz et al., 1991).

Parameters for the photosynthesis model include the maximum rates of carboxylation (V_{cmax}) and electron transport (J_{max}). These parameters vary seasonally due to the phenological state of the vegetation. These parameters were evaluated seasonally and spatially using optimization theory (Wang et al., 2017). Parameters for the conductance model include the Ball-Berry slope and intercept. Slope is set 13 for herbaceous vegetation and 9.5 for woody vegetation, respectively (Miner et al., 2017) (Miner et al., 2017). Intercept is set 0.01 umol·m^{-2}·s^{-1} (Duursma et al., 2019) with a multiplicative water stress factor $\sqrt{\mathrm{RH}^{\mathrm{VPD}/1000}}$.

The set of equations used to calculate evaporation is composed of nonlinear functions and is driven by drivers that possess non-Gaussian probability distributions, such as direct and diffuse solar radiation. To evaluate the expected values of these functions correctly (Ruel & Ayres, 1999) and with fidelity, we apply a two-layer (vegetation/soil) and dual source (sun-shade) model (Norman, 1982; Sinclair et al., 1976). We do not track soil moisture budget explicitly. Alternatively, we rely on short- and long-term coupling between soil moisture deficits, the LAI of the site, the vapor pressure deficit in the boundary layer, and evaporation rates. This assumption has been shown to work very well for producing accurate estimates of evaporation across the United States (Fisher et al., 2008; Gentine et al., 2016; Rigden & Salvucci, 2015). At this juncture we are disinclined to use satellite-based information on soil moisture, from such products from the Soil Moisture Active Passive Mission (Entekhabi et al., 2010), because it only senses a shallow layer, a few centimeters deep. And products from the Gravity Recovery and Climate Experiment (Famiglietti et al., 2011) are too coarse in time and space for this application.

2.2. Model Forcing Variables

This model is driven with a unique suite of land and atmospheric products that are derived from the Moderate Imaging Spectrometer (MODIS) on the Terra and Aqua satellites. Computations of the shortwave and longwave radiation components were forced with data from several MODIS products (MOD/MYD04_L2 aerosol, MOD/MYD06_L2 cloud, MOD/MYD07_L2 atmosphere profile, MOD/MYD11_L2 land surface temperature and emissivity, and MCD43D61 shortwave albedo).

Few modeling teams have used these separate data products in tandem because it requires one to preprocess the data and reproject them on a common geographical grid. We stress that combining these two complementary data sets is one of the unique strengths of this modeling approach as it produces more accurate radiation fields (Ryu et al., 2018).

Two snapshots are taken each day from the Terra and Aqua satellite platforms, and this information is upscaled to daily sum of evaporation using a simple cosine function (Ryu et al., 2012). At a given pixel, 1 to 5 km, forcing variables, such as temperature, radiation, humidity, albedo, and LAI, are evaluated (Jiang et al., 2017; Ryu, Kang, et al., 2008; Ryu et al., 2018).

Flux densities of shortwave global radiation (R_g), photosynthetically active radiation, and the diffuse component of photosynthetically active radiation were computed using a modified version of the Forest Light Environmental Simulator (Kobayashi & Iwabuchi, 2008). The radiative transfer model is one dimensional. It considers the scattering and absorption effects of clouds, aerosols, atmospheric pressure, temperature, and humidity on the transfer of photons through the atmosphere using a Monte Carlo photon tracing scheme. Broadband radiative flux densities were computed by integrating spectral radiation components evaluated at 20-nm interval between 300 and 700 nm and at 100-nm interval between 700 and 4,000 nm.

The atmospheric radiative transfer scheme was validated with surface radiation measurements from the Baseline Surface Radiation Network and FLUXNET flux tower networks (Ryu et al., 2018). The model produces estimates of daily integrated flux densities of incoming radiation that are highly correlated with surface measurements ($r^2 > 0.94$) and show little bias with measurements (< ±2%). In addition, the mean annual estimate of global radiation over the land surface (184 W/m^2) compared identically with an independent analysis based on land measurements (Wild et al., 2015).

MODIS, MOD15A2H, and MCD15A3H LAI products were filled and filtered using a simple time series analysis approach to minimize cloud contamination. They, along with a global dynamic clumping index maps derived from MODIS and MISR data (Chen et al., 2005; Wei & Fang, 2016), were used to calculate shortwave and longwave radiation components absorbed by sunlit/shade canopy and soil. Air temperature and dew point temperature from ERA-Interim reanalysis data (Dee et al., 2011) were merged with data derived from MOD/MYD07_L2 product to achieve high spatial (MODIS, 5 km) and temporal (ERA, 6-hourly) forcing fields.

Statewide averages of precipitation were extracted from the National Climatic Data Center, Climate at a Glance, database (https://www.ncdc.noaa.gov/cag). Evaporation calculations produced bioregions across the state were based on regional shapefiles that were obtained from a database created by the Interagency Natural Areas Coordinating Committee. USGS National Gap Analysis Program raster file containing vegetation information of California was used to generate the oak savanna raster and polygon files used in this project. USDA Cropland Data Layer raster files were clipped to cover the area of the state of California and ranging from 2008 to 2017. Because Cropland Data Layers are unavailable in California prior to 2008, we assume that the 2008 layer is representative of crop cover patterns from 2001 to 2007. This data set was used to extract cells by specific attributes and generate raster and shape files for almonds, grapes, pasture, and orchards.

All code and files required for the monthly extraction analysis are available in a Python Jupyter Notebook (https://ipython.org/notebook.html), which can be obtained freely through GitHub (https://github.com/daviddralle/CA-ET). BESS evaporation rasters are made publicly available through the Google Earth Engine platform (metadata at https://code.earthengine.google.com/?asset=users/daviddralle/bessv2; Google Earth Engine asset ID users/daviddralle/bessv2).

2.3. Model Evaluation and Intercomparisons

The BESS model has been evaluated against a global network of eddy covariance flux stations (Jiang & Ryu, 2016; Ryu et al., 2012) and machine learning products of spatial evaporation (Jung et al., 2010). The BESS evaporation products agreed well with data from 113 FLUXNET sites ($R^2 = 0.62$, bias = 0.1 mm/day) on eight daily scale and with the output of a machine learning product ($R^2 = 0.90$, bias = 0.1 mm/day) on annual scale. In addition, we compared computations of energy fluxes with eddy covariance measurements we have made across central California, near the 38th degree parallel. These data are from a mesonetwork of Ameriflux/FLUXNET sites that consist of oak savanna, an annual grassland, agricultural crops, irrigated pasture, and restored wetlands (Baldocchi et al., 2016; Baldocchi & Ma, 2013; Eichelmann et al., 2018; Ryu, Baldocchi, et al., 2008). Data from these comparisons are shown in section 3.

At the state scale, we compare BESS computations of evaporation with a hierarchy of models. One model is the MODIS evaporation product (MOD16; Mu et al., 2011; Zhang et al., 2010). This product forces an algorithm that evaluates the Penman-Monteith equation. It is evaluated on 8-day intervals and at 1-km resolution.

A second model is the Simplified Surface Energy Balance (SSEBop v4; Senay et al., 2007; Senay et al., 2011). It determines evaporation using remotely sensed energy balance including MODIS thermal imagery (Bastiaanssen et al., 1998). It operates at 1-km resolution and on 10-day intervals. Data are available at the United States Geological Survey Early Warning web site (https://earlywarning.usgs.gov/fews/product/458).

The third model is the Max Planck Institute of Biogeochemistry's global evaporation product (Jung et al., 2011). This product is derived from empirical upscaling of direct eddy covariance fluxes of latent heat produced by the FLUXNET network (Pastorello et al., 2016). Fluxes are computed on monthly time steps at 0.5° resolution using machine learning algorithms, gridded climate data, and remote sensing information.

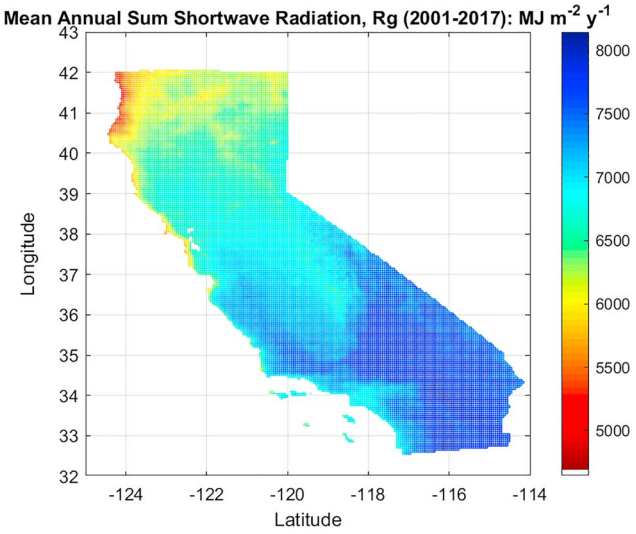

Figure 1. Map of global radiation (R_g) across California that is integrated over a year and averaged over the time series. Units are megaJoules per square meters per year.

These data are available from the Max Planck Data Portal (https://www.bgc-jena.mpg.de/geodb/projects/Home.php).

The fourth model is based on the Noah land surface model used in the Global Land Data Assimilation System, GLDAS,V2.1 (Rodell et al., 2004). Evaporation estimates are produced at 3-hr time steps and 0.25° resolution. These data are made available on the Google Earth Engine web site (https://developers.google.com/earth-engine/datasets/catalog/NASA_GLDAS_V021_NOAH_G025_T3H).

3. Results

3.1. Statewide Forcing Fields

To interpret the spatial-temporal variations in California evaporation, we first examine the statewide maps of variables that were used to compute, or evaluate, maps and time series of evaporative fluxes: solar radiation, net radiation, potential evaporation, and maximum LAI. These maps were produced by averaging or summing data over the course of a year and then averaging over the 2001–2017 time period.

Figure 1 shows the map of annually integrated, global solar radiation (R_g). The annually integrated, multiyear, and statewide average, flux density of incoming solar radiation is 7028 ± 90 MJ·m^{-2}·year^{-1}. Spatially, incoming solar radiation increases from 5,000 to 8,000 MJ·m^{-2}·year^{-1} across the north to south, west to east gradient.

For perspective, we compared our computations from a set of measurements from our mesonetwork of flux measurements sites that span across central California at about the 38° parallel (Eichelmann et al., 2018; Ryu, Baldocchi, et al., 2008). Table 1 shows that we computed an incident solar load on the order of 6,700 MJ·m^{-2}·year^{-1} for this latitude band, and we measured an average incident solar radiation load in the range between 6,600 and 6,800 MJ·m^{-2}·year^{-1}. The agreement between measured and modeled incoming global radiation is very strong and consistent with findings from the global test of the model (Ryu et al., 2018).

Evaporation is a function of the net radiation balance of the surface (Monteith, 1981). Figure 2 shows the map of annually integrated net radiation (R_n), where net radiation is the difference between incoming and outgoing shortwave and longwave radiation. Net radiation ranged between 2,000 and 4,000 MJ·m^{-2} year^{-1}, relative to a statewide average of 3,140 MJ·m^{-2} year^{-1}. The agricultural fields in the Central Valley, shrubland sites in the northeast, snow fields of the high Sierra Nevada mountains, and desert vegetation in the south experienced the lowest values of net radiation. This observation occurred because

Table 1
A Comparison of BESS Model Computations of Annually Integrated Global Radiation (R_g), Net Radiation (R_n), and evaporation (E) From 2001 to 2017 With Ecosystem Scale Observations Across a Network of Sites Near the 38th Parallel of California

	Vaira R_g (MJ·m^{-2}·year^{-1})	Tonzi R_g (MJ·m^{-2}·year^{-1})	Delta R_g (MJ·m^{-2}·year^{-1})	Vaira R_n (MJ·m^{-2}·year^{-1})	Tonzi R_n (MJ·m^{-2}·year^{-1})	Delta R_n (MJ·m^{-2}·year^{-1})	Vaira E (mm/year)	Tonzi E (mm/year)	Delta E (mm/year)
BESS computations									
Mean sum	6,775	6,787	6,714	2,967	2,956	3,256	468	476	717
Standard deviation	161	161	169	48	47	80	45	44	47
AmeriFlux measurements									
Mean sum	6,873	6,694	6,830	2,405	3,335	3,248	299	371	738
Standard deviation	286	178	299	262	272	490	40	60	125

Note. Field observations come from an oak savanna at the Tonzi Ranch (https://doi.org/10.17190/AMF/1245971), an annual grassland at the Vaira Ranch (https://doi.org/10.17190/AMF/1245984), and a pasture (https://doi.org/10.17190/AMF/1246094), corn (https://doi.org/10.17190/AMF/1246148), and alfalfa (https://doi.org/10.17190/AMF/1246149) field in the Sacramento-San Joaquin Delta. Data were gap filled and distributed with the FLUXNET 2015 data release. BESS = Breathing Earth System Simulator.

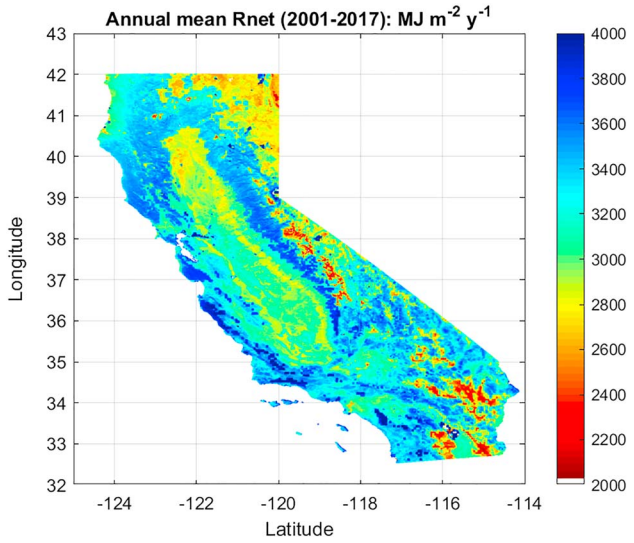

Figure 2. Map of net radiation (R_n) budget across California that is integrated over a year and averaged over the time series. Units are megaJoules per square meters per year.

they possess higher albedoes and/or surface temperatures. Conversely, evergreen forests that ring the Central Valley and reside on the coastal, Cascade, and Sierra Nevada mountain ranges possess the greatest net radiation budgets because they have relatively low albedos and surface temperatures (maps of albedo and surface temperature are shown in supporting information Figures S1 and S2, and a map of major vegetation groups of the State is shown in Figure S3.).

Our ability to model the net radiation field was good (Table 1). Across our central California mesonetwork of flux sites near the 38th degree latitude band, we modeled annual sums of net radiation flux densities that are on the order of 2,900 to 3,200 MJ·m^{-2}·year^{-1}. Over farm fields in the Delta, we typically measured a net radiation balance near 3,200 MJ·m^{-2}·year^{-1} and over the oak savanna on the Sierra Nevada foothills we measured net radiation that summed to about 3,300 MJ·m^{-2}·year^{-1}. Given, issues of spatial alignment between flux towers and satellite pixels, the agreement is favorable.

Potential evaporation sets the upper limit of water use by a landscape and is a value reached by well-watered vegetation with high LAIs. Figure 3 shows the map of annually integrated potential evaporation (PET). This variable was computed using the Priestley-Taylor equation (Priestley & Taylor, 1972), where PET = 1.26 $(s/(s + \gamma))$ R_n/λ, s is the slope of the saturation vapor pressure-temperature relation, γ is the psychrometric constant, and λ is latent heat of energy. The Priestley-Taylor equation is preferred as a measure of potential evaporation because it represents the evaporation from a freely evaporating surface and it incorporates feedbacks with the planetary boundary layer and its humidity (McNaughton & Spriggs, 1986); Figure S4, in supporting information, shows the theoretical response between latent heat exchange, normalized by its equilibrium rate, λE_{eq}, and the surface conductance (G_s); this normalized rate of evaporation approaches the value of the Priestley-Taylor constant, 1.26, when surface conductance exceeds 20 mm/s.

Wide swaths of the state are subject to potential evaporation demand that exceed a meter of water per year, on an area basis; the statewide average potential evaporation is 1,082 mm/year. This value, for state wide potential evaporation, is considerably lower than the previously published value of 1,344 mm/year; that value is referenced to evaporation from a well-watered grass according to the modified Penman equation (Hidalgo et al., 2005). It is noteworthy that the spatial fields of potential evaporation across the Central Valley, which consider the energy balance of the actual landscape, are lower than values of potential evaporation derived from functions that refer to evaporation from a reference field of green grass (Burt et al., 2002; Hidalgo et al., 2005). The biophysical features of these land use cover types and their management are reflected in the calculations of net radiation and potential evaporation presented here. Many of these fields are fallow or deciduous a significant fraction of the year, giving them higher albedos and surface temperatures than would be experienced over a reference green grass, when evaluated on an annual time scale (supporting information Figures S1 and S2). The BESS model also shows that the seasonally snow-covered regions of the Sierra Nevada mountains, with high albedo and a relatively short growing season, have the lowest values of potential evaporation.

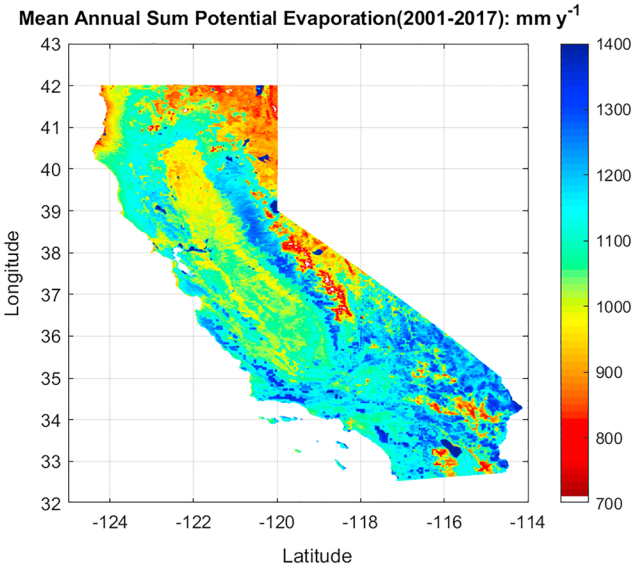

Figure 3. Map of annually integrated potential evaporation across California, computed with the Priestly-Taylor equation. Units are millimeter per year.

The source strength of evaporation scales with LAI. Consequently, regions with greater LAI are expected to experience greater amounts of evaporation. Conversely, regions with deficit rainfall are expected to sustain lower values of LAI and experience lower values of evaporative water use. Figure 4 shows the map of maximum LAI. Forests growing in wetter

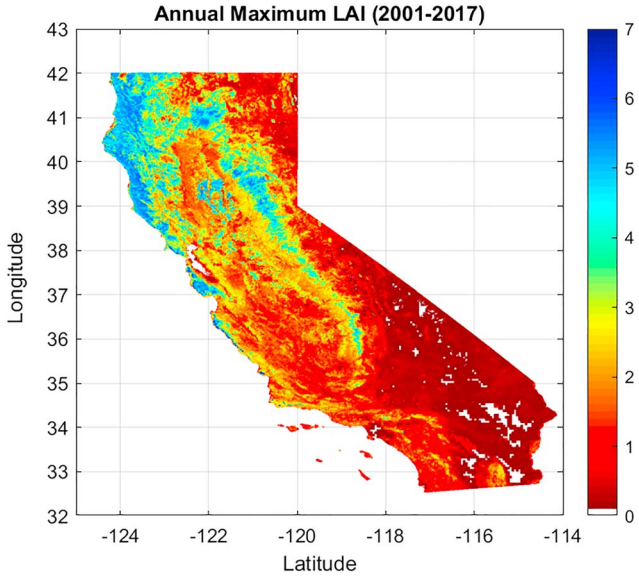

Figure 4. Map of maximum leaf area index across California. LAI = leaf area index.

climates of the Pacific north coast and subalpine elevations of the Sierra Nevada mountains and irrigated orchards in the Central Valley achieve closed canopies and LAIs up to 5 m^2/m^2. The drier landscapes of the state are occupied by sparser vegetation, having LAIs between 1 and 2 m^2/m^2. Maximum values of LAIs for many irrigated crops in the Central Valley are less than 3 m^2/m^2. This may seem lower than expected, given that these fields are intensively managed. However, farmers need to have spacing between plants to cultivate the fields, so moderate values of LAI (less than 3) are common for key perennial crops like grapes (Johnson et al., 2003; Kustas et al., 2018), walnuts (Patton et al., 2011), and almonds (Falk et al., 2013; Zarate-Valdez et al., 2012). Furthermore, the data in Figure 4 resemble spatial patterns and magnitudes of LAI derived from an independent study based on the simple ratio and the Advanced Very High Resolution Radiometer (Nikolov & Zeller, 2006).

3.2. Spatial-Temporal Evaporation Fields

Figure 5 shows the space and time-averaged map of annual evaporation computed across California by BESS for the MODIS observation period, 2001–2017. The statewide spatial and multiyear average of the annual sum of evaporation, determined pixel by pixel, is 393 ± 48 mm/year. The histogram of statewide, annual evaporation is bimodal and positively skewed, yielding a median of 359 mm/year (see supporting information Figure S5). These sums are 36% of potential evaporation.

Annual sums of evaporation experience strong west to east longitudinal, north to south latitudinal, and low to high elevation gradients in annual evaporative water use. In general, pixels with the highest evaporation, above 700 mm/year, are concentrated along the central and northwest coasts, which is home to the tall and evergreen temperate rain forests, across the subalpine forests of the northern and southern Sierra Nevada, the wine growing regions of the coast range, and in specific agricultural sectors of the Delta, in the middle Central Valley. Within the agricultural regions are fields that use 800 to 1,000 mm/year (Baldocchi et al., 2016; Drexler et al., 2008; Eichelmann et al., 2018; Kochendorfer et al., 2011). The ring of grasslands and oak savanna around the Central Valley evaporates 300 to 400 mm/year, which is on par with eddy covariance measurements over oak savanna and annual grasslands in this region (Baldocchi et al., 2004). Semiarid shrublands evaporate less than 200 mm/year. Deserts evaporate less than 100 mm/year. The hot, irrigated Imperial Valley, near the Mexican border, was detected to use less than 300 mm/year, when averaged over pixels 1 km in dimension. The complex mosaic of crops, their crop calendar, the physiological stress imposed by hot summer temperatures, and the fraction of land that may be fallow any given year contributed to a marked difference in the amount of evaporation for a given crop versus that for a wider agricultural region.

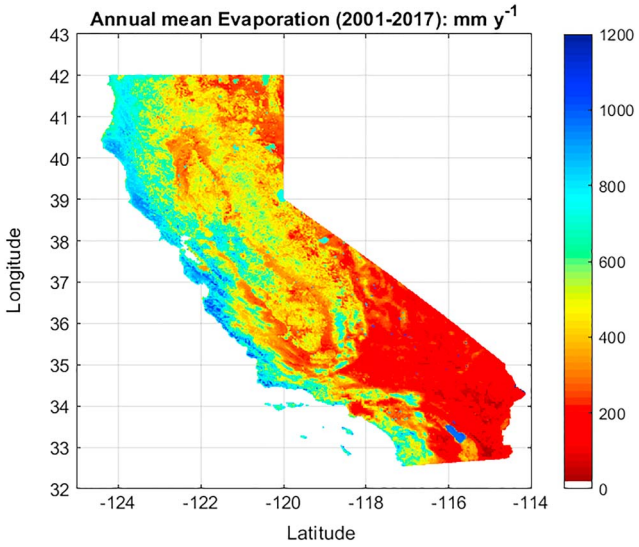

Figure 5. Map of annual evaporation (mm/year) across California, averaged over the period between the 2001 and 2017 calendar years. The *x* axis is degrees longitude, and the *y* axis is degrees longitude.

In Table 2 we report integrated averages and sums of annual water use for broad geographic regions in the state; monthly sums are shown in supporting information Figure S6. The lowest annual water use, under 200 mm/year, occurs over the Mojave and Colorado deserts. The highest regional water use occurs over the forests of the Klamath/North Coast (596 ± 13 mm/year) and the irrigated agriculture of the Delta and Bay Area (590 ± 20 mm/year). The irrigated agricultural fields in the Sacramento Valley, where water is relatively plentiful, and fields are flooded during the winter for water fowl, lost on average 421 ± 30 mm/year to evaporation. In contrast, the irrigated agriculture fields in the San Joaquin Valley, which are subject to restrictions in water delivery during droughts, evaporate less, for example, 374 ± 37 mm/year.

Table 2
Mean Annual Sums of Evaporation for Selected Geographic Regions; Regions Are Delimited in Supporting Information Figure S5

Regions	Mean mm/year	Standard deviation mm/year	km^3/year	Area (km^2)
Bay area/delta	590	20	15	25,430
Central Coast	494	41	16	32,333
Colorado Desert	177	20	4.9	27,654
Klamath/North Coast	596	13	34.7	58,161
Modoc	370	14	12.5	33,718
Mojave	217	27	17.6	81,305
Sacramento Valley	421	30	6.7	15,987
San Joaquin Valley	374	37	12.5	33,322
Sierra Nevada	396	24	29.4	74,193
South Coast	396	35	11.4	28,713
Total			160.8	423,970
Potential evaporation	1,087	14	460.8	423,970

The integrated amount of evaporation across the Sierra Nevada mountains is 396 ± 24. Eddy covariance measurements across the upper King River Basin of the southern range of the Sierra Nevada mountains are comparable; they were on the order of 429 mm/year (Goulden et al., 2012).

Irrigated agriculture is one of the largest users of water in California (Hanak et al., 2011). How much water is used by specific crops across wide areas? To better understand the spatial-temporal variation in evaporation across California, we parsed the statewide evaporation map into dominant climate and ecological regions using the Cropland Data Layer (Table 3).

Mean crop water use ranged between 400 and 584 mm/year, which was less than 53% of potential evaporation. Corn, a highly productive C_4, crop, used the most water on an area basis (584 ± 29 mm/year), followed by walnuts (509 mm/year) and almonds (481 ± 37 mm/year). Monthly variability of evaporation tended to be out of phase with potential evaporation, as hot, dry summer months hindered actual evaporation (supporting information Figure S7).

The year-to-year variability in annual evaporation and precipitation, averaged across the state, is shown in Figure 6. One key finding is the fact that the interannual variability in statewide evaporation is relatively small (±5%) and buffered from the high interannual variability in precipitation (±28%). This buffered response occurred despite the occurrence of extreme droughts (Seager et al., 2015) during this observation period. This finding is an indicator that native vegetation is well adapted to the booms and busts in rainfall and maintains a conservative posture in water use. It is only during extreme and prolonged drought when elevated plant mortality occurs.

Nor did we observe a time trend in annual evaporation or precipitation that was significantly different from zero. The linear regression between evaporation and time yielded a slope of −0.453 mm/year^2, r^2 equal to 0.0134, and P equal to 0.6402. The linear regression between precipitation and time yielded a slope of −1.533 mm/year^2, r^2 equal to 0.110, and P equal to 0.185.

Given that the standard deviation in state wide evaporation equals 48 mm/year, the 95% confidence interval of the slope of the time trends of evaporation must exceed 0.179 mm/year^2 or 1.79 mm/year per decade, to be significantly different than trends due to the propagation of random errors in computing the time series (see supporting information Figures S8 and S9).

Another notable feature of Figure 6 is the fact that evaporation exceeded precipitation during the driest calendar year, 2013. This is inferential evidence that many ecosystems were able to survive during this excessively dry period, in the short term, by tapping deeper sources of water. And those that did not experience elevated mortality the following years (Asner et al., 2015). We add that if we examine these results by water year, we do not see as much as an imbalance in 2013–2014.

Table 3
Mean Annual Sums of Evaporation for Selected Crops, Orchards, and Ecosystems

Crops	Mean (mm/year)	Standard deviation (mm/year)
Alfalfa	440	25
Almonds	484	32
Corn	587	21
Grapes	446	28
Grass	401	31
Walnuts	512	26
Oak savanna	399	54
Potential evaporation	1,087	14

3.3. Sensitivity of Evaporation to Forcing Variables

Numerous climate projections expect more evaporative water use by vegetation with a warming climate on the assumption that saturation vapor pressure of the surface will increase and force a stronger gradient with the atmosphere (Hayhoe et al., 2004). The BESS model considers feedbacks between demand and supply.

To examine why are we not experiencing temporal trends in evaporation across California, we compared the time series of key drivers of evaporation, precipitation, air temperature, and LAI (Figure 7). To facilitate intercomparison, these climate data were reported relative to the mean over the 1895 to 2017 time period and normalized by their standard

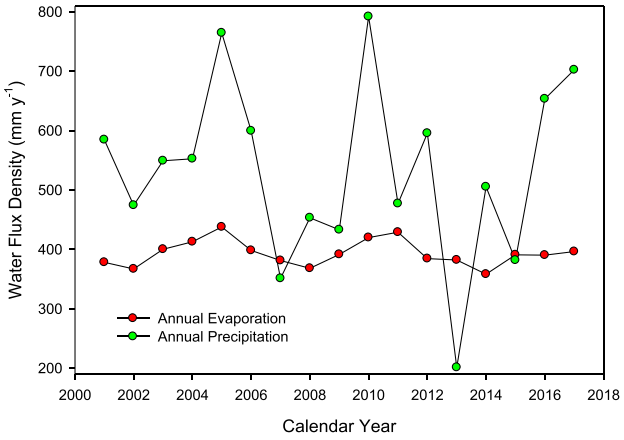

Figure 6. Year-to-year variation in annual evaporation and precipitation, for the calendar year across California.

deviation. The slopes of the trends for normalized deviations in precipitation, maximum LAI, and evaporation were not significantly different from zero (precipitation: slope = −0.0118, P = 0.821; ET: slope = 0.0894; P = 0.765; LAI: slope = −0.0400; P = 0.4374). Only the trend in temperature was significantly greater than zero (slope = −0.0155; P = 0.0379).

4. Discussion

4.1. Hypothesis Tests

Hypothesis 1 postulated that year-to-year variability in statewide evaporation is sensitive to booms and busts in rainfall. We found that the year-to-year variability in statewide evaporation was relatively insensitive to booms and busts in rainfall; the slope of the linear regression between annual precipitation and evaporation is on the order of 0.08. This relative insensitivity occurred in part because native ecosystems have adapted their structural and functional attributes to a highly variable rainfall regime. Many native plants are resilient to frequent drought because they are able to extract water from deeper sources in the water column. And where tree mortality occurred, juveniles and other understory vegetation resumed evaporation once rains returned.

Hypothesis 2 postulated that a positive temporal trend in statewide evaporation should be observed due to a warming climate. We falsified this hypothesis because we did not calculate a temporal trend in statewide evaporation over 17 years that was significantly different from zero. In a warmer and drier world partial stomatal closure, more radiative loss of energy by the surface and reduction in LAI may counteract against an expected gradient in humidity that is predicted with simpler land surface models, embedded into climate simulations (Monteith, 1981); we discuss these feedbacks in more detail below. Our study does not remove the possibility of a positive trend in evaporation being detected in the future, with more warming.

Hypothesis 3 postulated that agricultural crops water use is closely related to the amount defined as potential evaporation and vastly exceeds amounts evaporated by native species. Our computations of agricultural evaporation, at 1-km scale, were nearly half of potential evaporation. But can we truly conclude we falsified this hypothesis?

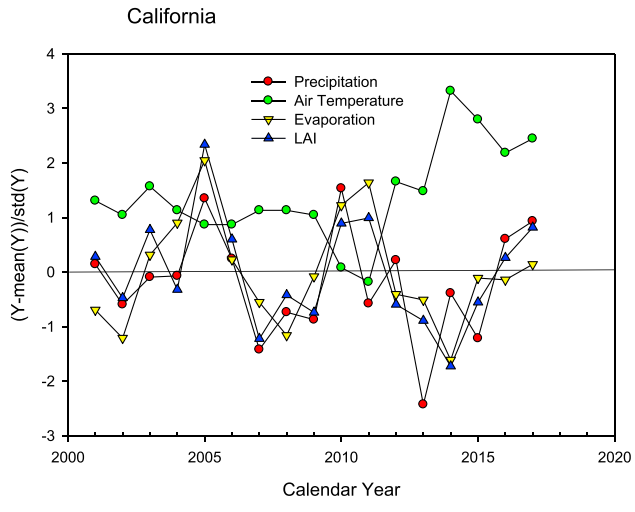

Figure 7. Trends in precipitation, temperature, maximum leaf area index, and evaporation across California. The climate data were reported relative to the mean over the 1895 to 2017 time period. Trends were computed for the 2001 to 2017 time period. The slopes of the trends for precipitation, maximum leaf area index, and evaporation were not significant from zero. The trend in temperature was significantly greater than zero.

One study estimated evaporative water use of crops as a fraction of potential evaporation from a well-watered grass or evaporation pan times a seasonally varying crop coefficients (Allen, 2000; Burt et al., 2005; Snyder et al., 2005). They estimated that agricultural evaporative water use in California was on the order of 825 mm/year; this area-based estimate was based on 30.8 km^3 (25 million acre-feet) used by 3.75 million ha (9.3 million acres; Burt et al., 2002).

A second study inferred that gross and net water use by irrigated agriculture is on the order of 1,143 and 935 mm/year, respectively (Hanak et al., 2011); these calculations are based on 40.7 km^3 (33 million acre-feet) of gross water, and 33.2 km^3 (27 million acre-feet) of net water use is distributed across 3.56 million ha (8.80 million acre) of irrigated farmland.

These older literature values may be biased high. First, they refer to water use by individual fields, not the mosaic of fields that comprise a 1-km pixel. Second, they are tied to estimates of reference evaporation from well water grass which is on the order of 1,344 ± 70 mm/year (Hidalgo et al., 2005). In comparison, our estimates of potential evaporation, using the Priestley-Taylor equation and explicit computations of net radiation, are on the order of 1,080 mm/year. And it is known that farmers may apply more water than is needed by the plants and soil, because excess water is needed to push salts through the root system or it is captured as water runoff (Hanak et al., 2017).

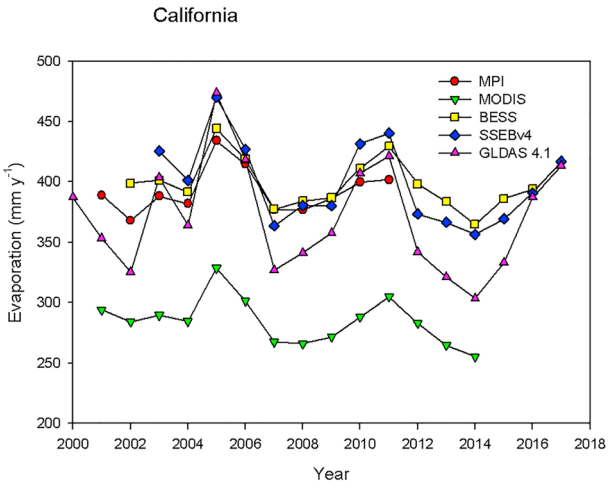

Figure 8. Validation of the BESS model with the Max Planck Institute (MPI) product, which is based on networks of flux towers and machine learning methods to produce gridded fluxes (Jung et al., 2011), the MODIS evaporation product (Zhang et al., 2010), the Simple Surface Energy Balance Model, SSEBv4 (Senay et al., 2011), and Global Land Data Assimilation System, GLDAS-2.1 (Rodell et al., 2004). BESS = Breathing Earth System Simulator.

We also acknowledge that our calculated sums of evaporation from orchards are lower than eddy covariance measurements (1036 mm/year) and simulations (900 to 1,100 mm/year) based on the ACASA-WRF model (Falk et al., 2013); ACASA is a higher-order closure model that considers wind, turbulence, and radiation fields within a multilayered canopy and uses similar coupled carbon, water, and energy flux algorithms, as applied here.

On the other hand, a new and independent study of evaporation across the irrigated crops of the Central Valley, using Morton's complementary evaporation method (Morton, 1983), estimates that annual evaporation is on the order of 369 ± 62 mm/year (Szilagyi & Jozsa, 2018), which is close to our calculations. It is also consistent with regional estimates of evaporation across the Central Valley computed with GLDAS (406 ± 50 mm/year) and SSEB (489 ± 51 mm/year; see Supporting Information Figures S10, S11, and S12). And the computations of evaporation over crops in the Sacramento-San Joaquin Delta are in general agreement with the eddy covariance fluxes we have measured (Eichelmann et al., 2018).

Based on the results from the literature and multiple models, we conclude that evaporation evaluated at relatively large (1 km) pixel scales is less than maximum evaporation from individual fields in that pixel, thereby falsifying Hypothesis 3.

4.2. Comparisons of Statewide Evaporation With Other Metrics

There is no perfect way to test the performance of model calculations at annual and statewide scales (Oreskes et al., 1994). Yet it is instructive to compare our statewide calculations of annual evaporation with other measures to bound random and systematic bias errors.

One statewide water budget, based on the CALVIN model, distributes 246 km^3 of mean annual statewide precipitation into 102 km^3 of gross water use, 78.9 km^3 of net water use, and 86.3 km^3 of unimpaired water availability (e.g., discharge and infiltration; Hanak et al., 2011). Given that the area of the state is 423,970 km^2, this volumetric sum translates to an area-averaged annual gross water flux of 241 mm/year, a value mostly attributed to evaporation. In comparison, BESS estimates that 161 km^3 of water is evaporated across the State on an annual basis (Table 2).

Figure 8 shows a comparison of statewide averages of evaporation between BESS and a hierarchy of land-atmosphere models. MPI model estimates mean, statewide annual evaporation to be 392 ± 19 mm/year. MPI method fits flux measurement from a global network of towers to interpolate evaporation in time and space (Jung et al., 2011). The estimate of statewide evaporation with the NASA MODIS Evaporation product (Mu et al., 2011; Zhang et al., 2010) equals 284 ± 19 mm/year. An extraction of annual sums of evaporation from the Simple Energy Balance Model (Senay et al., 2011) yields a mean of 399 ± 34 mm/year. And evaporation derived from GLDAS is 371 ± 45 mm/year; it is also noteworthy that the GLDAS evaporation product showed no trend in evaporation.

We find that the mechanistic BESS model matches the estimates of evaporation at the state scale that were produced by the machine learning model and the land surface model within 7%. On the other hand, the NASA MODIS evaporation and water-budget evaporation products greatly underestimated (by about 100 mm/year), while the SSEB model agrees with BESS within a millimeter per year. This comparison gives us confidence that BESS is performing as well as other models used by the community.

One has to be careful about achieving "the right answer for the wrong reason". We must remember that each model scheme has strengths and weaknesses. The Noah-WRF model in the GLADAS data set is operating at coarse space scales and does not consider coupling between carbon and water fluxes. A recent paper compared the Noah-WRF model with eddy flux measurements from the Vaira Ranch in California (Chang et al., 2018), and this paper reported severe errors in Noah-WRF's ability to simulate measured values of sensible and latent heat.

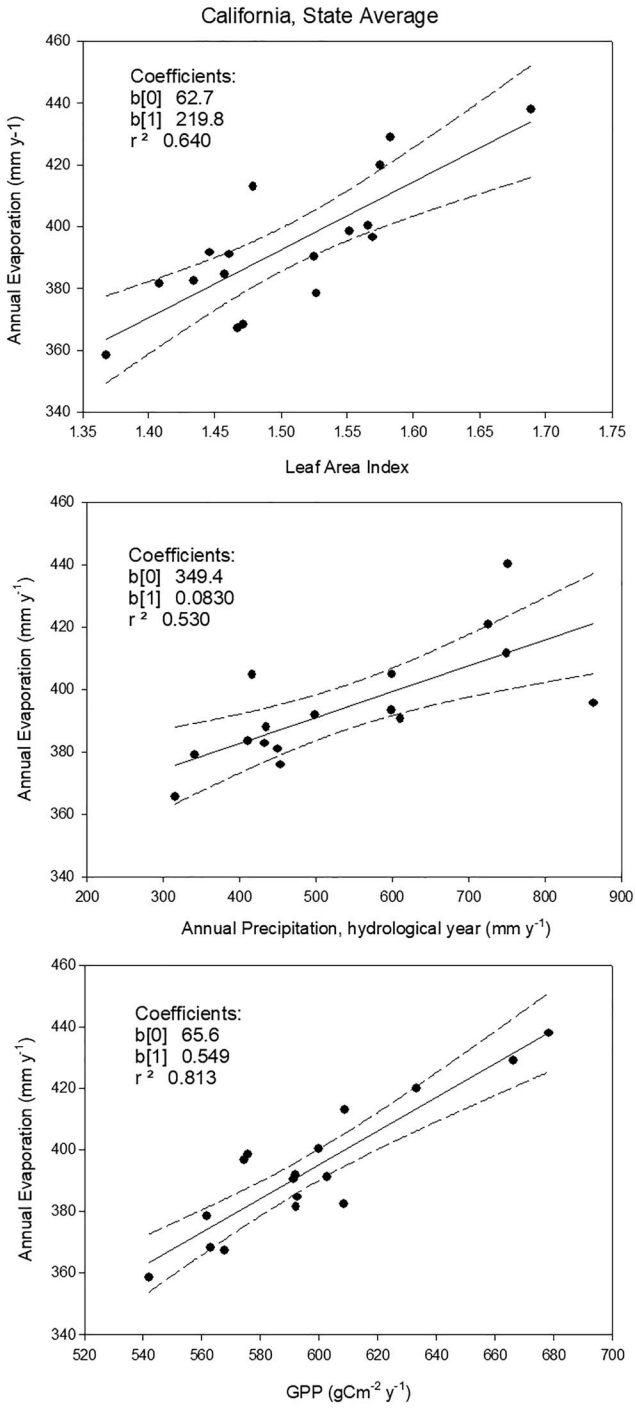

Figure 9. The dependence of annual evaporation on maximum leaf area index (top), annual precipitation (middle), and gross primary production (bottom).

Inspection of the evaporation map produced by SSEB (supporting information Figure S11) shows strong regional differences with BESS. The developers of SSEB warn on their web site:

> "despite the improved accuracy, the ET product is still more reliable in a relative sense as in anomalies for drought. The absolute accuracy can vary from region-to region; thus users are encouraged to evaluate and determine a one-time bias correction for water budget applications."We leave this section on the note that BESS evaporation products are consistent with a range of sums produced by a hierarchy of models at the state scale. On the other hand, there remains much uncertainty and variability among models on how much water is evaporated across representative climate and ecological zones.

4.3. Sources of Variability

What is the sensitivity of statewide evaporation to changes in dominant environmental drivers we can assess or measure? Figure 9 shows the dependency of interannual variation in evaporation on maximum LAI, precipitation, and gross primary productivity. First, we find that 64% of interannual variability in evaporation is explained by LAI, which varies year to year due to the amount of rain, fires, and planting decisions. Second, we find that 83% of the variability in evaporation is explained by gross primary productivity. This metric reflects the role of atmospheric humidity deficits on stomatal conductance and integrates the impact of LAI. Third, 53% of the variation in evaporation is directly explained by hydrological year precipitation, and the coupling, defined by the slope, is only 0.083; only 24% of the variation in evaporation was explained by variations in calendar year precipitation. The low year-to-year variability in modeled evaporation rates is consistent with values we have measured over annual grasslands (Ryu, Baldocchi, et al., 2008) and over an oak savanna Ameriflux site in California (Baldocchi & Ma, 2013). This behavior is also a common feature of Mediterranean-type vegetation (Joffre & Rambal, 1993), as they are not able to increase transpiring leaf area fast enough during the wet years and are adapted to frequent water deficits by establishing a sparse canopy with relatively low LAI.

We also mapped the sensitivity of evaporation (dE) to a suite of environmental variables, vapor pressure deficit (VPD), temperature (T), solar radiation (R_g), and LAI.

$$\mathrm{d}E = c_1 \cdot \mathrm{dVPD} + c_2 \cdot \mathrm{d}T + c_3 \cdot \mathrm{d}Rg + c_4 \cdot \mathrm{dLAI}$$

We analyzed the multivariate regression pixel by pixel with a partial least squares regression on four variables, removed trends, and normalized each pixel by the standard deviation of its multiyear population. All variables were normalized (z scored) so they are unitless and comparable. Figure 10 shows the maps the sensitivity coefficients (c_1 ... c_4) for each respective variable and the r^2 for the multivariate linear regression.

Across most of the state, these four variables explained most of the variation in evaporation. This sensitivity analysis helps explain how and why feedbacks among these drivers dampen the response of evaporation over time to temperature. We see that the effects of incremental increases in temperature were countered by incremental decreases in vapor pressure deficits. The sunny deserts of the south were relatively insensitive to solar radiation, while the cloudy and wetter north showed positive sensitivity to solar radiation. Evaporation for most pixels across the state responded positively to increases in LAI.

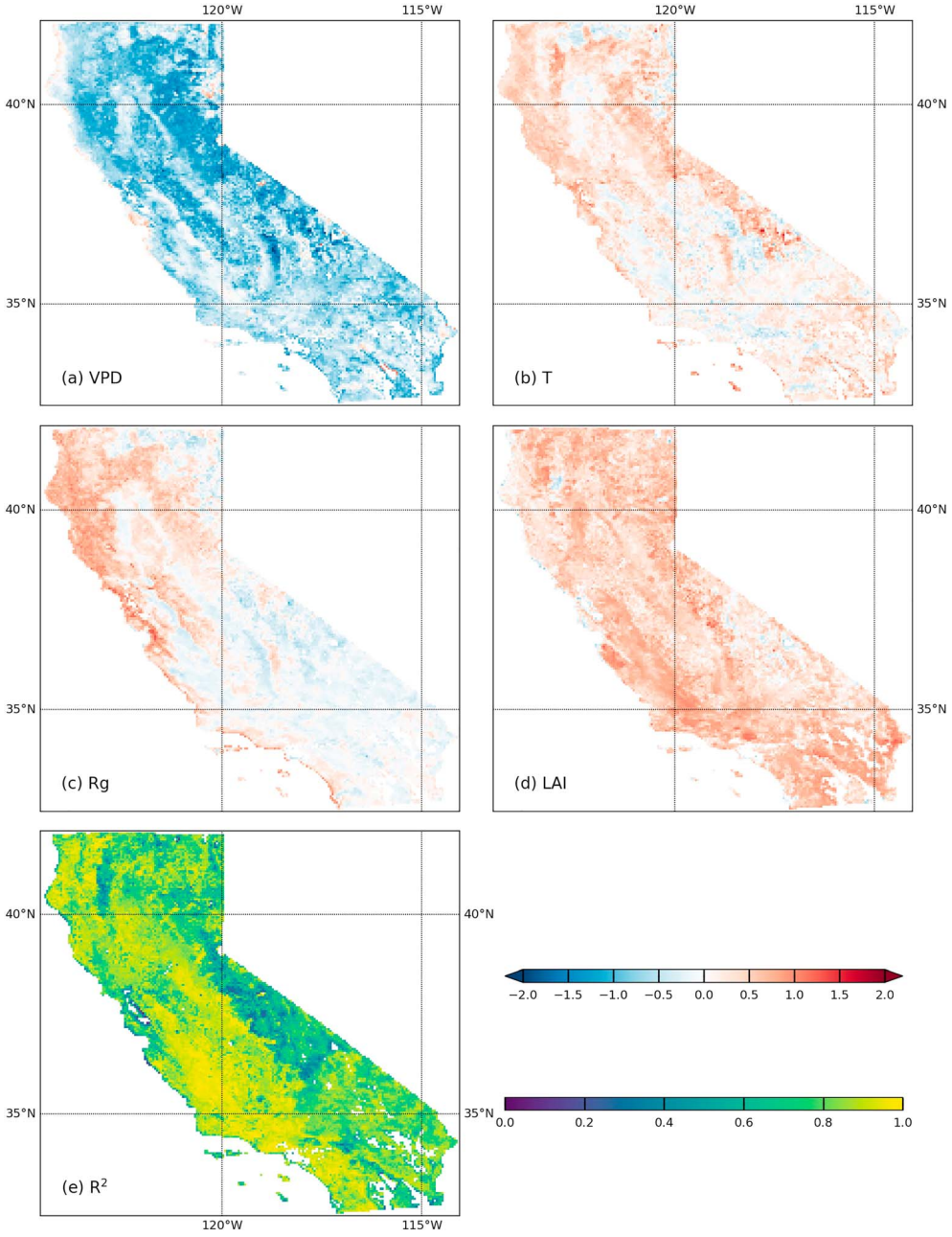

Figure 10. Sensitivity of evaporation to variations in driving variables based on an analysis of a mulivariate regression for each pixel. (a) Vapor pressure deficit, (b) air temperature, (c) solar radiation, (d) leaf area index, and (e) coefficient of determination. VPD = vapor pressure deficit; LAI = leaf area index.

The BESS model can simulate the impacts of wet and dry climates on evaporation through its simulation of the surface conductance. Surface conductance is modulated by such factors as LAI, vapor pressure deficits, photosynthesis, and photosynthetic capacity, which in turn scale with leaf nitrogen and soil moisture (Kelliher et al., 1995). How surface conductance varies across California is shown in supporting information Figure S13. The annual mean value of surface conductance ranges between 1 and 10 mm/s. The low values of surface conductance, superimposed on the response function shown in supporting information Figure S4, help explain why evaporation across much of the state is much below potential evaporation on an annual time scale. As inferred from supporting information Figure S4, the ratio between $\lambda E/\lambda E_{eq}$ will range between 0.2 and 1 as surface conductance ranges between 1 and 10 mm/s.

This mechanistic BESS model also informed us that the highest evaporation totals occurred along the North Coast, despite the fact that this region experiences more fog, clouds, and rain than other parts of the state. While its potential evaporation may be relatively lower than sunnier regions (1,100 vs. 1.300 mm/year), these ecosystems were able to achieve higher sums of actual evaporation, compared to vegetation in the more xeric regions of the state, because they are more effective absorbers of solar radiation (they are optically darker and maintain high LAIs), they experience a long growing season, they achieve the highest surface conductances (supporting information Figure S13), and they had access to deep, unsaturated stores of water in fractured weathered bedrock keeps stomata open (Rempe & Dietrich, 2018). It is possible that an underestimation of evaporation from the temperate rain forests in the northwest may account for some of the discrepancy between our statewide residual water budgets and past published results.

This long-term analysis also gives us some insight as to how evaporation across the state responded to the severe 2013 drought (Griffin & Anchukaitis, 2014), when statewide precipitation was 201 or 331 mm below the 17-year ensemble mean. Our analysis shows a lag or legacy effect as we observed the lowest rates of evaporation during 2014 (358 mm/year). During 2014, both annual evaporation and LAI were 9% lower than the long-term means (393 mm/year). One contribution to lower water use in 2014 was the decision to put 121 kha in fallow across the San Joaquin Valley (Hanak et al., 2017). Another factor was the loss of 104 kha of forest from the Tuolumne Rim Fire, near Yosemite during the autumn of 2013.

4.4. Sources of Uncertainty

Models like BESS possess a set of uncertainties and random and systematic errors that depend upon time and space scales. Some errors may be additive and others compensating.

First, there are errors and uncertainties associated with the model structure and complexity (Medlyn et al., 2005). BESS has the positive attribute that it captures the coupling between photosynthesis, stomatal conductance, and surface energy balance using a set of nonlinear functions. It is necessary to compute the expected value of a nonlinear function rather than the function of the mean value of the independent variable (Ruel & Ayres, 1999). BESS minimizes this type of error by adopting a dual source (sun/shade), coupled photosynthesis/energy balance model, as has been advocated in the literature (Norman, 1982; Sinclair et al., 1976).

We recognize that our computations may experience some error during the dry season because we omitted information on soil moisture, but there is evidence that information on vapor pressure deficits can compensate (Rigden & Salvucci, 2015; Stocker et al., 2018). Other errors that may arise stem from the assumption that the canopy is a sun/shade big leaf. We know that multilayer, higher-order closure Eulerian and random walk Lagrangian models, that treat the canopy microclimate in more detail, are more accurate (Baldocchi, 1992; Falk et al., 2013; Vogel et al., 1995). But differences between computations of evaporation that do and do not consider vertical variations of humidity in the canopy are small (Baldocchi, 1992; Chang et al., 2018).

Second, there are errors and uncertainties associated with the meteorological drivers (light, temperature, and humidity), LAI, plant functional types (Medlyn et al., 2005), their representativeness at 1-km space scale (Raupach, 1991), and from a single midday acquisition (Ryu et al., 2012). For example, 0.5 m^2/m^2 uncertainty in statewide average LAI can alter annual statewide evaporation by 108 mm/year.

Third, there are errors associated with the grid scale and spatial abstraction of the land surface. By operating at 1-km pixel resolution, we attempt to address nonlinearities that are associated with coarser (10- to 50-km resolution) scale land surface models like Noah (Ek et al., 2003; Rodell et al., 2004). In practice, we lose data when clouds are present. Consequently, additional biases and errors can arise by the need interpolate and gap fill to compute daily and annual sums (Ryu et al., 2012). We also assume a flat Earth, which may affect the radiation balance on complex topography of the Sierra Nevada, Cascade, and Coastal mountains.

Fourth, there are errors associated with the specification of structural and functional information. It is well known that LAI, detected from remote sensing, saturates when LAI is high (Sellers, 1985). There is also error in designating plant functional types as C_3 and C_4 crops and due to the year-to-year variation in vegetation fields from farming practices, land use change, and fires. We know many fields (over 240, 000 hectares) are corn, a C4 plant, and this effect is ignored.

Fifth, model algorithms are sensitive to errors in the choice of parameters. Parameters for photosynthetic capacity, for example, will differ on leaves at the top and bottom of a canopy. They will also vary with time of year (Osuna et al., 2015). Scaling photosynthetic parameters with leaf traits is a new and improved way to assign them for a given pixel (Van Bodegom et al., 2012).

4.5. Impacts on Water Decisions and Management

From an operational perspective, the water budget of the California is very much out of balance and uncertain. There is more demand for water from its natural and human stakeholders than is available (Hanak et al., 2011). This has led to several negative environmental problems or unintended consequences. First, the excessive drafting of ground water in Central Valley has caused large-scale soil subsidence (Famiglietti et al., 2011; Faunt et al., 2016). Second, the redistribution of water from the north to the south has caused declines in water quality and fish population (Hanak et al., 2011). Subsidies to water, which have enabled interior desert valleys to bloom, have also led to inefficient practices such as the production of low-value irrigated forage crops and placement of golf courses where potential evaporation is extreme (Hanak et al., 2011). Furthermore, irrigation of soils in the Central Valley causes salts to accumulate (Schoups et al., 2005). And insufficient supplies of water during drought have forced many farmers to fallow their farmland; over 136 kha of farm land was in fallow across the San Joaquin Valley in 2014 (Hanak et al., 2017).

The intent of this model computation and spatial-temporal analysis on actual evaporation from natural and managed landscapes is to give water managers better information on how to share water among legitimate stakeholders during wet and dry years, using a high-resolution, bottom-up, mechanistic, biophysical model, as opposed to the top-down, large-scale, residual analysis that is often used. One key finding is that annual water use across California is steadier than the highly variable inputs of water from rainfall would infer. Access to water stored in soil, saprolite, and bedrock helps buffer this temporal variability in annual evaporation of native forests in some portions of the State (Garcia & Tague, 2015; Miller et al., 2010; Rempe & Dietrich, 2018). Another key finding is a new, hopefully, and better estimate of statewide and regional evaporation which policy makers can use to make decisions. At present, they make decisions on the basis of a large-scale, top-down water budget that infer net (78.9 km^3/year) and gross (102 km^3/year) water use across the state on an annual basis (Hanak et al., 2011); gross water use is the sum of evaporation and return flow; net water use is the sum of evaporation and nonrecoverable flow. We can compare our results with these metrics by multiplying the mean flux densities of precipitation and evaporation that we computed by land area. Over the 2001–2017 period, we estimate that the state receives on average about 219 km^3/year of water as precipitation and it evaporates 161 km^3/year of water. This leaves a residual of 58 km^3, which would be lost as by runoff to the ocean, lakes, and reservoirs from the rivers and infiltration to aquifers. This implies that more water is being lost statewide by evaporation, than has been estimated, so there may be less residual water available for other ecosystem and public services.

With regard to the agricultural regions of the state, our model estimates suggest that the crops are using less water than has been assumed. This analysis shows that spatial-temporal integration of evaporation across many of the irrigated regions of California does not reach the extremely high sums of potential evaporation (1,000 to 1,400 mm/year; Hidalgo et al., 2005). If true, at 1-km scale, this is relatively good news given the scarce amount and multiple demands for this water.

It is our assessment that many agricultural fields do not meet potential evaporation on an annual basis for a variety of reasons. They are fallow for a sizable fraction of the year; they only attain full canopy cover for a short period, they suffer physiological heat and soil moisture stress during the extremely hot summer, and maximum rates of evaporation occur for only short periods during their growing season. For example, our direct eddy covariance measurements over irrigated alfalfa show that extreme heat of the later summer Central Valley causes the system to experience stomatal closure and reduced actual evaporation, despite the high potential evaporation rates (Eichelmann et al., 2018). We would expect this summer time heat stress effect to be even greater for the vast amounts of alfalfa grown in the much hotter Imperial Valley. Therefore, we ask: Are we overirrigating our crops on a landscape basis, given the complicated mosaic of land use and a variable crop calendar, which alters phenology?

Inefficiencies in the application of water, via flood, furrow, and sprinkler irrigation, leakage and evaporative losses across the canal transmission systems, access to cheap and subsidized water, losses by soil

evaporation, and the need to flush the root zone for salts may be some reasons why conventional water use by crops has been relatively high, up to now. Conventional estimates of potential evaporation seem biased high, too, compared to our estimates of potential evaporation. Further work is needed to determine if farmers can apply less water, through drip irrigation, without incurring deleterious effects. If true, this could provide energy and water savings by reducing pumping, the amount of water applied. It could also have benefits by providing more water to ecosystem services and refilling aquifers.

4.6. Future Directions

We concede that the BESS model is based on a certain set of assumptions, in order to execute the model using satellite remote sensing. From our experience conducting this case study, we can identify several features that are needed to improve and refine the BESS model for improved and routine application in California. Better radiation fields could be computed if the model considers topography. Higher spatial resolution information of land use will give us better information on crop management mosaics. For example, in the Central Valley we need better information on where C_4 crops like corn and sorghum exist, as this affects computations of photosynthesis and stomatal conductance. Future versions of the model could be improved with incorporating information on soil moisture and vapor pressure deficit fields and information on rooting depth. Future analyses on the integrative effects of large fires on the water budget of the State are warranted, too.

5. Conclusion

We used a biophysical model driven by satellite remote sensing to produce a new multiyear map of annual evaporation sums across California. We find that annual sums of evaporation are relatively steady (±5%) given the high interannual variation in precipitation (±27%). We also compute lower sums of evaporative water use for the Central Valley than prior estimates that are tied to potential evaporation, due to the complex spatial mosaic and seasonality of crop management.

Overall, we find that potential evaporation is about 300 mm/year less than conventional than past assessments and that crops are using between 100 and 200 mm less water per year than anticipated from past studies that inferred water use from estimates of potential evaporation of well-watered grass. On the other hand, statewide, we find that more water is being evaporated compared to past assessments that estimate net and gross water use from the residual of the water balance or use simpler models driven with satellite information. Hence, as a statewide level there may be less residual water than previously assumed.

This new information may help water managers to plan and share water use among cities, ecosystems, and agriculture better and more equitably during series of wet and dry years.

Acknowledgments
We thank Gabriella de sa Queen for assistance in mapping the crops and ecosystems during early phase of this work. This research was supported in part by the California Agricultural Extension Station, a Big Ideas grant from the College of Natural Resources, and a contract from the California Department of Water Resources. Funding for AmeriFlux core site data was provided by the U.S. Department of Energy's Office of Science. We also thank the team of technicians, postdocs, and graduate students from the Biometeorology Lab, who have helped collect and process eddy flux data from our mesonetwork of sites across California. The National Research Foundation of Korea (NRF-2014R1A2A1A11051134) supported the development of the BESS model. The National Science Foundation CZP EAR-1331940 for the Eel River Critical Zone Observatory supported the efforts of DND.

References

Allen, R. G. (2000). Using the FAO-56 dual crop coefficient method over an irrigated region as part of an evapotranspiration intercomparison study. *Journal of Hydrology*, *229*(1–2), 27–41. https://doi.org/10.1016/S0022-1694(99)00194-8

Anderson, J., Chung, F., Anderson, M., Brekke, L., Easton, D., Ejeta, M., et al. (2008). Progress on incorporating climate change into management of California's water resources. *Climatic Change*, *87*(S1), 91–108. https://doi.org/10.1007/s10584-007-9353-1

Anderson, M. C., Kustas, W. P., & Norman, J. M. (2007). Upscaling flux observations from local to continental scales using thermal remote sensing. *Agronomy Journal*, *99*(1), 240. https://doi.org/10.2134/agronj2005.0096S

Asner, G. P., Brodrick, P. G., Anderson, C. B., Vaughn, N., Knapp, D. E., & Martin, R. E. (2015). Progressive forest canopy water loss during the 2012–2015 California drought. *Proceedings of the National Academy of Sciences*, *113*(2), E249–E255.

Baldocchi, D., Knox, S., Dronova, I., Verfaillie, J., Oikawa, P., Sturtevant, C., et al. (2016). The impact of expanding flooded land area on the annual evaporation of rice. *Agricultural and Forest Meteorology*, *223*, 181–193. https://doi.org/10.1016/j.agrformet.2016.04.001

Baldocchi, D., & Ma, S. Y. (2013). How will land use affect air temperature in the surface boundary layer? Lessons learned from a comparative study on the energy balance of an oak savanna and annual grassland in California, USA. *Tellus Series B-Chemical and Physical Meteorology*, *65*(1). https://doi.org/10.3402/tellusb.v65i0.19994

Baldocchi, D. D. (1992). A Lagrangian random walk model for simulating water vapor, CO_2, and sensible heat flux densities and scalar profiles over and within a soybean canopy. *Boundary Layer Meteorology*, *61*(1-2), 113–144. https://doi.org/10.1007/BF02033998

Baldocchi, D. D., & Meyers, T. (1998). On using eco-physiological, micrometeorological and biogeochemical theory to evaluate carbon dioxide, water vapor and trace gas fluxes over vegetation: A perspective. *Agricultural and Forest Meteorology*, *90*(1–2), 1–25. https://doi.org/10.1016/S0168-1923(97)00072-5

Baldocchi, D. D., Xu, L., & Kiang, N. (2004). How plant functional-type, weather, seasonal drought, and soil physical properties alter water and energy fluxes of an oak-grass savanna and an annual grassland. *Agricultural and Forest Meteorology*, *123*(1–2), 13–39. https://doi.org/10.1016/j.agrformet.2003.11.006

Ball, J. T., Woodrow, I. E., & Berry, J. A. (1987). In J. Biggins (Ed.), *Progress in photosynthesis research: Volume 4 proceedings of the VIIth international congress on photosynthesis* (pp. 221–224). Dordrecht, Netherlands: Springer.

Bastiaanssen, W. G. M., Menenti, M., Feddes, R. A., & Holtslag, A. A. M. (1998). A remote sensing surface energy balance algorithm for land (SEBAL). 1. Formulation. *Journal of Hydrology*, *212-213*, 198–212. https://doi.org/10.1016/S0022-1694(98)00253-4

Budyko, M. I. (1974). *Climate and life*. New York, NY: Academic Press.

Burt, C., Mutziger, A., Howes, D. and Solomon, K. (2002) Evaporation from irrigated agricultural land in California. Report No. 02-001.

Burt, C. M., Mutziger, A. J., Allen, R. G., & Howell, T. A. (2005). Evaporation research: Review and interpretation. *Journal of Irrigation and Drainage Engineering-Asce*, *131*(1), 37–58. https://doi.org/10.1061/(ASCE)0733-9437(2005)131:1(37)

Chang, K.-Y., Paw, U. K. T., & Chen, S.-H. (2018). Canopy profile sensitivity on surface layer simulations evaluated by a multiple canopy layer higher order closure land surface model. *Agricultural and Forest Meteorology*, *252*, 192–207. https://doi.org/10.1016/j.agrformet.2018.01.027

Chen, J. M., Menges, C. H., & Leblanc, S. G. (2005). Global mapping of foliage clumping index using multi-angular satellite data. *Remote Sensing of Environment*, *97*(4), 447–457. https://doi.org/10.1016/j.rse.2005.05.003

Collatz, G. J., Ball, J. T., Grivet, C., & Berry, J. A. (1991). Physiological and environmental regulation of stomatal conductance, photosynthesis and transpiration: A model that includes a laminar boundary layer. *Agricultural and Forest Meteorology*, *54*(2–4), 107–136. https://doi.org/10.1016/0168-1923(91)90002-8

Dee, D. P., Uppala, S. M., Simmons, A. J., Berrisford, P., Poli, P., Kobayashi, S., et al. (2011). The ERA-Interim reanalysis: Configuration and performance of the data assimilation system. *Quarterly Journal of the Royal Meteorological Society*, *137*(656), 553–597. https://doi.org/10.1002/qj.828

Dettinger, M. D., Ralph, F. M., Das, T., Neiman, P. J., & Cayan, D. R. (2011). Atmospheric rivers, floods and the water resources of California. *Water*, *3*(2), 445–478. https://doi.org/10.3390/w3020445

Diffenbaugh, N. S., Swain, D. L., & Touma, D. (2015). Anthropogenic warming has increased drought risk in California. *Proceedings of the National Academy of Sciences*, *112*(13), 3931–3936. https://doi.org/10.1073/pnas.1422385112

Dralle, D. N., Hahm, W. J., Rempe, D. M., Karst, N. J., Thompson, S. E., & Dietrich, W. E. (2018). Quantification of the seasonal hillslope water storage that does not drive streamflow. *Hydrological Processes*, *32*(13), 1978–1992. https://doi.org/10.1002/hyp.11627

Draper, A. J., Jenkins, M. W., Kirby, K. W., Lund, J. R., & Howitt, R. E. (2003). Economic-engineering optimization for California water management. *Journal of Water Resources Planning and Management-Asce*, *129*(3), 155–164. https://doi.org/10.1061/(ASCE)0733-9496(2003)129:3(155)

Drexler, J. Z., Anderson, F. E., & Snyder, R. L. (2008). Evapotranspiration rates and crop coefficients for a restored marsh in the Sacramento-San Joaquin Delta, California, USA. *Hydrological Processes*, *22*(6), 725–735. https://doi.org/10.1002/hyp.6650

Duursma, R. A., Blackman, C. J., Lopéz, R., Martin-StPaul, N. K., Cochard, H., & Medlyn, B. E. (2019). On the minimum leaf conductance: Its role in models of plant water use, and ecological and environmental controls. *New Phytologist*, *221*(2), 693–705. https://doi.org/10.1111/nph.15395

Eichelmann, E., Hemes, K. S., Knox, S. H., Oikawa, P. Y., Chamberlain, S. D., Sturtevant, C., et al. (2018). The effect of land cover type and structure on evapotranspiration from agricultural and wetland sites in the Sacramento–San Joaquin River Delta, California. *Agricultural and Forest Meteorology*, *256–257*, 179–195.

Ek, M. B., Mitchell, K. E., Lin, Y., Rogers, E., Grunmann, P., Koren, V., et al. (2003). Implementation of Noah land surface model advances in the National Centers for Environmental Prediction operational mesoscale Eta model. *Journal of Geophysical Research*, *108*(D22), 8851. https://doi.org/10.1029/2002JD003296

Entekhabi, D., Njoku, E. G., O'Neill, P. E., Kellogg, K. H., Crow, W. T., Edelstein, W. N., et al. (2010). The Soil Moisture Active Passive (SMAP) mission. *Proceedings of the IEEE*, *98*(5), 704–716. https://doi.org/10.1109/JPROC.2010.2043918

Falk, M., Pyles, R. D., Ustin, S. L., Paw, U. K. T., Xu, L., Whiting, M. L., et al. (2013). Evaluated crop evapotranspiration over a region of irrigated orchards with the improved ACASA–WRF model. *Journal of Hydrometeorology*, *15*(2), 744–758.

Famiglietti, J. S., Lo, M., Ho, S. L., Bethune, J., Anderson, K. J., Syed, T. H., et al. (2011). Satellites measure recent rates of groundwater depletion in California's Central Valley. *Geophysical Research Letters*, *38*, L03403. https://doi.org/10.1029/2010GL046442

Farquhar, G. D., Caemmerer, S. V., & Berry, J. A. (1980). A biochemical-model of photosynthetic CO_2 assimilation in leaves of C-3 species. *Planta*, *149*(1), 78–90. https://doi.org/10.1007/BF00386231

Faunt, C. C., Sneed, M., Traum, J., & Brandt, J. T. (2016). Water availability and land subsidence in the Central Valley, California, USA. *Hydrogeology Journal*, *24*(3), 675–684. https://doi.org/10.1007/s10040-015-1339-x

Fisher, J. B., Melton, F., Middleton, E., Hain, C., Anderson, M., Allen, R., et al. (2017). The future of evapotranspiration: Global requirements for ecosystem functioning, carbon and climate feedbacks, agricultural management, and water resources. *Water Resources Research*, *53*, 2618–2626. https://doi.org/10.1002/2016WR020175

Fisher, J. B., Tu, K. P., & Baldocchi, D. D. (2008). Global estimates of the land–atmosphere water flux based on monthly AVHRR and ISLSCP-II data, validated at 16 FLUXNET sites. *Remote Sensing of Environment*, *112*(3), 901–919. https://doi.org/10.1016/j.rse.2007.06.025

Garcia, E. S., & Tague, C. L. (2015). Subsurface storage capacity influences climate–evapotranspiration interactions in three western United States catchments. *Hydrology and Earth System Sciences*, *19*(12), 4845–4858. https://doi.org/10.5194/hess-19-4845-2015

Gentine, P., Chhang, A., Rigden, A., & Salvucci, G. (2016). Evaporation estimates using weather station data and boundary layer theory. *Geophysical Research Letters*, *43*, 11,661–611,670. https://doi.org/10.1002/2016GL070819

Gentine, P., D'Odorico, P., Lintner, B. R., Sivandran, G., & Salvucci, G. (2012). Interdependence of climate, soil, and vegetation as constrained by the Budyko curve. *Geophysical Research Letters*, *39*, L19404. https://doi.org/10.1029/2012GL053492

Goulden, M. L., Anderson, R. G., Bales, R. C., Kelly, A. E., Meadows, M., & Winston, G. C. (2012). Evapotranspiration along an elevation gradient in California's Sierra Nevada. *Journal of Geophysical Research*, *117*, G03028. https://doi.org/10.1029/2012JG002027

Griffin, D., & Anchukaitis, K. J. (2014). How unusual is the 2012–2014 California drought? *Geophysical Research Letters*, *41*, 9017–9023. https://doi.org/10.1002/2014GL062433

Hanak, E., Lund, J., Arnold, B., Escriva-Bou, A., Gray, B., Green, S., et al. (2017). *Water stress and a changing San Joaquin Valley*. San Francisco, CA: Public Policy Institute of California.

Hanak, E., Lund, J., Dinar, A., Gray, B., Howitt, R., Mount, J., et al. (2011). *Managing California's water: From conflict to reconciliation*. San Francisco, CA: Public Policy Institute of California.

Hart, Q. J., Brugnach, M., Temesgen, B., Rueda, C., Ustin, S. L., & Frame, K. (2009). Daily reference evapotranspiration for California using satellite imagery and weather station measurement interpolation. *Civil Engineering and Environmental Systems*, *26*(1), 19–33. https://doi.org/10.1080/10286600802003500

Hayhoe, K., Cayan, D., Field, C., Frumhoff, P. C., Maurer, E. P., Miller, N. L., et al. (2004). Emissions pathways, climate change and impacts on California. *Proceedings of the National Academy of Sciences of the United States of America*, *101*(34), 12,422–12,427. https://doi.org/10.1073/pnas.0404500101

Hidalgo, H., Cayan, D., & Dettinger, M. (2005). Sources of variability of evapotranspiration in California. *Journal of Hydrometeorology*, *6*(1), 3–19. https://doi.org/10.1175/JHM-398.1

Iacobellis, S. F., Cayan, D. R., Abatzoglou, J. T., & Mooney, H. (2016). *Climate*. Oakland: University of California Press.

Ichii, K., Wang, W., Hashimoto, H., Yang, F., Votava, P., Michaelis, A. R., & Nemani, R. R. (2009). Refinement of rooting depths using satellite-based evapotranspiration seasonality for ecosystem modeling in California. *Agricultural and Forest Meteorology*, *149*(11), 1907–1918. https://doi.org/10.1016/j.agrformet.2009.06.019

Jarvis, P. G., & McNaughton, K. G. (1986). Stomatal control of transpiration: Scaling up from leaf to region. *Advances in Ecological Research*, *15*, 1–49. https://doi.org/10.1016/S0065-2504(08)60119-1

Jiang, C., & Ryu, Y. (2016). Multi-scale evaluation of global gross primary productivity and evapotranspiration products derived from Breathing Earth System Simulator (BESS). *Remote Sensing of Environment*, *186*, 528–547. https://doi.org/10.1016/j.rse.2016.08.030

Jiang, C., Ryu, Y., Fang, H., Myneni, R., Claverie, M., & Zhu, Z. (2017). Inconsistencies of interannual variability and trends in long-term satellite leaf area index products. *Global Change Biology*, *23*(10), 4133–4146. https://doi.org/10.1111/gcb.13787

Jin, Y., Randerson, J. T., & Goulden, M. L. (2011). Continental-scale net radiation and evapotranspiration estimated using MODIS satellite observations. *Remote Sensing of Environment*, *115*(9), 2302–2319. https://doi.org/10.1016/j.rse.2011.04.031

Joffre, R., & Rambal, S. (1993). How tree cover influences the water balance of Mediterranean rangelands. *Ecology*, *74*(2), 570–582. https://doi.org/10.2307/1939317

Johnson, L. F., Roczen, D. E., Youkhana, S. K., Nemani, R. R., & Bosch, D. F. (2003). Mapping vineyard leaf area with multispectral satellite imagery. *Computers and Electronics in Agriculture*, *38*(1), 33–44. https://doi.org/10.1016/S0168-1699(02)00106-0

Jung, M., Reichstein, M., Ciais, P., Seneviratne, S. I., Sheffield, J., Goulden, M. L., et al. (2010). Recent decline in the global land evapotranspiration trend due to limited moisture supply. *Nature*, *467*(7318), 951–954. https://doi.org/10.1038/nature09396

Jung, M., Reichstein, M., Margolis, H. A., Cescatti, A., Richardson, A. D., Arain, M. A., et al. (2011). Global patterns of land-atmosphere fluxes of carbon dioxide, latent heat, and sensible heat derived from eddy covariance, satellite, and meteorological observations. *Journal of Geophysical Research*, *116*, G00J07. https://doi.org/10.1029/2010JG001566

Kelliher, F. M., Leuning, R., Raupach, M. R., & Schulze, E.-D. (1995). Maximum conductances for evaporation from global vegetation types. *Agricultural and Forest Meteorology*, *73*(1–2), 1–16. https://doi.org/10.1016/0168-1923(94)02178-M

Kobayashi, H., & Iwabuchi, H. (2008). A coupled 1-D atmosphere and 3-D canopy radiative transfer model for canopy reflectance, light environment, and photosynthesis simulation in a heterogeneous landscape. *Remote Sensing of Environment*, *112*(1), 173–185. https://doi.org/10.1016/j.rse.2007.04.010

Kochendorfer, J., Castillo, E. G., Haas, E., Oechel, W. C., Paw, U., & K.T. (2011). Net ecosystem exchange, evapotranspiration and canopy conductance in a riparian forest. *Agricultural and Forest Meteorology*, *151*(5), 544–553. https://doi.org/10.1016/j.agrformet.2010.12.012

Kustas, W. P., Anderson, M. C., Alfieri, J. G., Knipper, K., Torres-Rua, A., Parry, C. K., et al. (2018). The Grape Remote sensing Atmospheric Profile and Evapotranspiration eXperiment (GRAPEX). *Bulletin of the American Meteorological Society.*, *99*(9), 1791–1812. https://doi.org/10.1175/BAMS-D-16-0244.1

McNaughton, K. G., & Spriggs, T. W. (1986). A mixed-layer model for regional evaporation. *Boundary-Layer Meteorology*, *34*(3), 243–262. https://doi.org/10.1007/BF00122381

Medlyn, B. E., Robinson, A. P., Clement, R., & McMurtrie, R. E. (2005). On the validation of models of forest CO_2 exchange using eddy covariance data: Some perils and pitfalls. *Tree Physiology*, *25*(7), 839–857. https://doi.org/10.1093/treephys/25.7.839

Miller, G. R., Chen, X., Rubin, Y., Ma, S., & Baldocchi, D. D. (2010). Groundwater uptake by woody vegetation in a semiarid oak savanna. *Water Resources Research*, *46*, W10503. https://doi.org/10.1029/2009WR008902

Miner, G. L., Bauerle, W. L., & Baldocchi, D. D. (2017). Estimating the sensitivity of stomatal conductance to photosynthesis: A review. *Plant, Cell & Environment*, *40*, 1214–1238. https://doi.org/10.1111/pce.12871

Monson, R., & Baldocchi, D. (2014). *Terrestrial biosphere-atmosphere fluxes*. Cambridge: Cambridge University Press. https://doi.org/10.1017/CBO9781139629218

Monteith, J. L. (1965). Evaporation and the environment. *Symposium of the Society of Exploratory Biology*, *19*, 205–234.

Monteith, J. L. (1981). Evaporation and surface-temperature. *Quarterly Journal of the Royal Meteorological Society*, *107*(451), 1–27. https://doi.org/10.1002/qj.49710745102

Morton, F. I. (1983). Operational estimates of areal evapotranspiration and their significance to the science and practice of hydrology. *Journal of Hydrology*, *66*(1–4), 1–76. https://doi.org/10.1016/0022-1694(83)90177-4

Mu, Q., Zhao, M., & Running, S. W. (2011). Improvements to a MODIS global terrestrial evapotranspiration algorithm. *Remote Sensing of Environment*, *115*(8), 1781–1800. https://doi.org/10.1016/j.rse.2011.02.019

Nikolov, N., & Zeller, K. (2006). Efficient retrieval of vegetation leaf area index and canopy clumping factor from satellite data to support pollutant deposition assessments. *Environmental Pollution*, *141*(3), 539–549. https://doi.org/10.1016/j.envpol.2005.08.059

Norman, J. M. (1982). In J. L. Hatfield (Ed.), *Biometeorology in integrated pest management* (pp. 65–99). San Diego, CA: Academic Press.

Oreskes, N., Shrader-Frechette, K., & Belitz, K. (1994). Verification, validation, and confirmation of numerical models in the Earth Sciences. *Science*, *263*(5147), 641–646. https://doi.org/10.1126/science.263.5147.641

Osuna, J. L., Baldocchi, D. D., Kobayashi, H., & Dawson, T. E. (2015). Seasonal trends in photosynthesis and electron transport during the Mediterranean summer drought in leaves of deciduous oaks. *Tree Physiology*, *35*(5), 485–500. https://doi.org/10.1093/treephys/tpv023

Pastorello, G., Papale, D., Chu, H., Trotta, C., Agarwal, D., Canfora, E. C., et al. (2016) The FLUXNET2015 Dataset: The longest record of global carbon, water, and energy fluxes is updated. Eos Trans. AGU.

Patton, E. G., Horst, T. W., Sullivan, P. P., Lenschow, D. H., Oncley, S. P., Brown, W. O. J., et al. (2011). The canopy horizontal array turbulence study. *Bulletin of the American Meteorological Society*, *92*(5), 593–611. https://doi.org/10.1175/2010BAMS2614.1

Paw, U. K. T., & Gao, W. G. (1988). Applications of solutions to non-linear energy budget equations. *Agricultural and Forest Meteorology*, *43*(2), 121–145. https://doi.org/10.1016/0168-1923(88)90087-1

Priestley, C. H. B., & Taylor, R. J. (1972). On the assessment of surface heat flux and evaporation using large-scale parameters. *Monthly Weather Review*, *100*(2), 81–92. https://doi.org/10.1175/1520-0493(1972)100<0081:OTAOSH>2.3.CO;2

Raupach, M. R. (1991). Vegetation-atmosphere interaction in homogeneous and heterogeneous terrain—Some implications of mixed-layer dynamics. *Vegetatio*, *91*(1–2), 105–120. https://doi.org/10.1007/BF00036051

Rempe, D. M., & Dietrich, W. E. (2018). Direct observations of rock moisture, a hidden component of the hydrologic cycle. *Proceedings of the National Academy of Sciences*, *115*(11), 2664–2669. https://doi.org/10.1073/pnas.1800141115

Rigden, A. J., & Salvucci, G. D. (2015). Evapotranspiration based on equilibrated relative humidity (ETRHEQ): Evaluation over the continental US. *Water Resources Research*, *51*, 2951–2973. https://doi.org/10.1002/2014WR016072

Rodell, M., Houser, P. R., Jambor, U., Gottschalck, J., Mitchell, K., Meng, C.-J., et al. (2004). The global land data assimilation system. *Bulletin of the American Meteorological Society*, *85*(3), 381–394. https://doi.org/10.1175/BAMS-85-3-381

Rosenzweig, M. L. (1968). Net primary productivity of terrestrial communities—Prediction from climatological data. *American Naturalist*, *102*(923), 67–74. https://doi.org/10.1086/282523

Ruel, J. J., & Ayres, M. P. (1999). Jensen's inequality predicts effects of environmental variation. *Trends in Ecology & Evolution*, *14*(9), 361–366. https://doi.org/10.1016/S0169-5347(99)01664-X

Ryu, Y., Baldocchi, D. D., Black, T. A., Detto, M., Law, B. E., Leuning, R., et al. (2012). On the temporal upscaling of evapotranspiration from instantaneous remote sensing measurements to 8-day mean daily-sums. *Agricultural and Forest Meteorology*, *152*, 212–222. https://doi.org/10.1016/j.agrformet.2011.09.010

Ryu, Y., Baldocchi, D. D., Kobayashi, H., van Ingen, C., Li, J., Black, T. A., et al. (2011). Integration of MODIS land and atmosphere products with a coupled-process model to estimate gross primary productivity and evapotranspiration from 1 km to global scales. *Global Biogeochemical Cycles*, *25*, GB4017. https://doi.org/10.1029/2011GB004053

Ryu, Y., Baldocchi, D. D., Ma, S., & Hehn, T. (2008). Interannual variability of evapotranspiration and energy exchange over an annual grassland in California. *Journal of Geophysical Research*, *113*, D09104. https://doi.org/10.1029/2007JD009263(D9)

Ryu, Y., Jiang, C., Kobayashi, H., & Detto, M. (2018). MODIS-derived global land products of shortwave radiation and diffuse and total photosynthetically active radiation at 5 km resolution from 2000. *Remote Sensing of Environment*, *209*, 812–825.

Ryu, Y., Kang, S., Moon, S.-K., & Kim, J. (2008). Evaluation of land surface radiation balance derived from moderate resolution imaging spectroradiometer (MODIS) over complex terrain and heterogeneous landscape on clear sky days. *Agricultural and Forest Meteorology*, *148*(10), 1538–1552. https://doi.org/10.1016/j.agrformet.2008.05.008

Schoups, G., Hopmans, J. W., Young, C. A., Vrugt, J. A., Wallender, W. W., Tanji, K. K., & Panday, S. (2005). Sustainability of irrigated agriculture in the San Joaquin Valley, California. *Proceedings of the National Academy of Sciences of the United States of America*, *102*(43), 15,352–15,356. https://doi.org/10.1073/pnas.0507723102

Seager, R., Hoerling, M., Schubert, S., Wang, H., Lyon, B., Kumar, A., et al. (2015). Causes of the 2011–14 California Drought. *Journal of Climate*, *28*(18), 6997–7024. https://doi.org/10.1175/JCLI-D-14-00860.1

Sellers, P. J. (1985). Canopy reflectance, photosynthesis and transpiration. *International Journal of Remote Sensing*, *6*(8), 1335–1372. https://doi.org/10.1080/01431168508948283

Sellers, P. J., Dickinson, R. E., Randall, D. A., Betts, A. K., Hall, F. G., Berry, J. A., et al. (1997). Modeling the exchanges of energy, water, and carbon between continents and the atmosphere. *Science*, *275*(5299), 502–509. https://doi.org/10.1126/science.275.5299.502

Senay, G. B., Budde, M., Verdin, J. P., & Melesse, A. M. (2007). A coupled remote sensing and simplified surface energy balance approach to estimate actual evapotranspiration from irrigated fields. *Sensors*, *7*(6), 979–1000. https://doi.org/10.3390/s7060979

Senay, G. B., Budde, M. E., & Verdin, J. P. (2011). Enhancing the Simplified Surface Energy Balance (SSEB) approach for estimating landscape ET: Validation with the METRIC model. *Agricultural Water Management*, *98*(4), 606–618. https://doi.org/10.1016/j.agwat.2010.10.014

Sinclair, T. R., Murphy, C. E., & Knoerr, K. R. (1976). Development and evaluation of simplified models for simulating canopy photosynthesis and transpiration. *Journal of Applied Ecology*, *13*(3), 813–829. https://doi.org/10.2307/2402257

Snyder, R. L., Orang, M., Matyac, S., & Grismer, M. E. (2005). Simplified estimation of reference evapotranspiration from Pan evaporation data in California. *Journal of Irrigation and Drainage Engineering*, *131*(3), 249–253. https://doi.org/10.1061/(ASCE)0733-9437(2005)131:3(249)

Sorooshian, S., Li, J., Hsu, K. L., & Gao, X. (2011). How significant is the impact of irrigation on the local hydroclimate in California's Central Valley? Comparison of model results with ground and remote-sensing data. *Journal of Geophysical Research*, *116*, D06102. https://doi.org/10.1029/2010JD014775

Stephenson, N. (1998). Actual evapotranspiration and deficit: Biologically meaningful correlates of vegetation distribution across spatial scales. *Journal of Biogeography*, *25*(5), 855–870. https://doi.org/10.1046/j.1365-2699.1998.00233.x

Stocker, B. D., Zscheischler, J., Keenan, T. F., Prentice, I. C., Peñuelas, J., & Seneviratne, S. I. (2018). Quantifying soil moisture impacts on light use efficiency across biomes. *New Phytologist*, *218*(4), 1430–1449. https://doi.org/10.1111/nph.15123

Swain, D. L., Langenbrunner, B., Neelin, J. D., & Hall, A. (2018). Increasing precipitation volatility in twenty-first-century California. *Nature Climate Change*, *8*(5), 427–433. https://doi.org/10.1038/s41558-018-0140-y

Szilagyi, J., & Jozsa, J. (2018). Evapotranspiration trends (1979–2015) in the Central Valley of California, USA: Contrasting tendencies during 1981–2007. *Water Resources Research*, *54*, 5620–5635. https://doi.org/10.1029/2018WR022704

Van Bodegom, P. M., Douma, J. C., Witte, J. P. M., Ordonez, J. C., Bartholomeus, R. P., & Aerts, R. (2012). Going beyond limitations of plant functional types when predicting global ecosystem-atmosphere fluxes: Exploring the merits of traits-based approaches. *Global Ecology and Biogeography*, *21*(6), 625–636. https://doi.org/10.1111/j.1466-8238.2011.00717.x

Vogel, C. A., Baldocchi, D. D., Luhar, A. K., & Rao, K. S. (1995). A comparison of a hierarchy of models for determining energy balance components over vegetation canopies. *Journal of Applied Meteorology*, *34*(10), 2182–2196. https://doi.org/10.1175/1520-0450(1995)034<2182:ACOAHO>2.0.CO;2

Wang, H., Prentice, I. C., Keenan, T. F., Davis, T. W., Wright, I. J., Cornwell, W. K., et al. (2017). Towards a universal model for carbon dioxide uptake by plants. *Nature Plants*, *3*(9), 734–741. https://doi.org/10.1038/s41477-017-0006-8

Wang, Y. P., Baldocchi, D., Leuning, R. A. Y., Falge, E. V. A., & Vesala, T. (2007). Estimating parameters in a land-surface model by applying nonlinear inversion to eddy covariance flux measurements from eight FLUXNET sites. *Global Change Biology*, *13*(3), 652–670. https://doi.org/10.1111/j.1365-2486.2006.01225.x

Wei, S., & Fang, H. (2016). Estimation of canopy clumping index from MISR and MODIS sensors using the normalized difference hotspot and darkspot (NDHD) method: The influence of BRDF models and solar zenith angle. *Remote Sensing of Environment*, *187*, 476–491. https://doi.org/10.1016/j.rse.2016.10.039

Wild, M., Folini, D., Hakuba, M. Z., Schar, C., Seneviratne, S. I., Kato, S., et al. (2015). The energy balance over land and oceans: An assessment based on direct observations and CMIP5 climate models. *Climate Dynamics*, *44*(11–12), 3393–3429. https://doi.org/10.1007/s00382-014-2430-z

Wood, E. F., Roundy, J. K., Troy, T. J., Beek, L. P. H. V., Bierkens, M. F. P., Blyth, E., et al. (2011). Hyperresolution global land surface modeling: Meeting a grand challenge for monitoring Earth's terrestrial water. *Water Resources Research*, *47*, W05301. https://doi.org/10.1029/2010WR010090

Zarate-Valdez, J. L., Whiting, M. L., Lampinen, B. D., Metcalf, S., Ustin, S. L., & Brown, P. H. (2012). Prediction of leaf area index in almonds by vegetation indexes. *Computers and Electronics in Agriculture*, *85*, 24–32. https://doi.org/10.1016/j.compag.2012.03.009

Zhang, K., Kimball, J. S., Nemani, R. R., & Running, S. W. (2010). A continuous satellite-derived global record of land surface evapotranspiration from 1983 to 2006. *Water Resources Research*, *46*, W09522. https://doi.org/10.1029/2009WR008800

Zhang, K., Kimball, J. S., & Running, S. W. (2016). A review of remote sensing based actual evapotranspiration estimation. *Wiley Interdisciplinary Reviews: Water*, *3*(6), 834–853. https://doi.org/10.1002/wat2.1168